

Browse ▾

My Settings ▾

Get Help ▾

Subscribe

All ▾

Enter keywords or phrases (Note: Searches metadata only by default. A search for 'smart grid' = 'smart AND grid')



Search within Publication

Advanced Search

| Other Search Options ▾

Browse Conferences > Progress in Electromagnetic Re... > 2018 Progress in Electromagnet... ?

## Progress in Electromagnetic Research Symposium (PIERS)

Copy Persistent Link

Browse Title List

Sign up for Conference Alerts

Proceedings

All Proceedings

Popular

2018 Progress in Electromagnetics Research Symposium (PIERS-Toyama)

DOI: 10.23919/PIERS-Toyama43567.2018

Search within results



Per Page: 25 ▾

| Export ▾

| Email Selected Results ▾

Showing 1-25 of 472

Refine

Author ▾

Affiliation ▾

Select All on Page

Sort By: Sequence ▾

2018 Progress In Electromagnetics Research Symposium (PIERS | Toyama)



Publication Year: 2018, Page(s): 1 - 1

▶ Abstract (158 Kb)

2018 Progress In Electromagnetics Research Symposium (PIERS | Toyama)



Publication Year: 2018 Page(s): 1 - 1

Need  
Full-Text

access to IEEE Xplore  
for your organization

Feedback

# 2018 Progress In Electromagnetics Research Symposium (PIERS — Toyama)

Copyright and Reprint Permission

© 2018 The Institute of Electronics, Information and Communication Engineer (IEICE). Personal use of this material is permitted. However, permission to reprint/republish this material for advertising or promotional purposes or for creating new collective works for resale or redistribution to servers or lists, or to reuse any copyrighted component of this work in other works must be obtained from the IEICE. As copyright holder for the PIERS 2018 Toyama Proceedings (abstracts and full-length papers), the IEICE grants the IEEE the nonexclusive, irrevocable, royalty-free worldwide rights to publish, sell, and distribute the copyrighted work for the Conference named above and any content derived from the copyrighted work in any format or media without restriction.

IEEE Catalog Number: CFP18C18-ART  
ISBN: 978-4-88552-315-1 C3855

## **THE ELECTROMAGNETICS ACADEMY**

The Progress in Electromagnetics Research Symposium (PIERS) is sponsored by The Electromagnetics Academy.

The Electromagnetics Academy is devoted to academic excellence and the advancement of research and relevant applications of the electromagnetic theory and to promoting educational objectives of the electromagnetics profession. PIERS provides an international forum for reporting progress and advances in the modern development of electromagnetic theory and its new and exciting applications.

Founded by the late Professor Jin Au Kong (1942–2008) of MIT in 1989, The Electromagnetics Academy is a non-profit organization registered in USA.

### **PIERS Founding Chair:**

Jin Au Kong, MIT, USA

### **President of The Electromagnetics Academy:**

Professor Leung Tsang, University of Michigan, USA

## **JOURNAL: PROGRESS IN ELECTROMAGNETICS RESEARCH**

Progress In Electromagnetics Research (PIER) publishes peer-reviewed original and comprehensive articles on all aspects of electromagnetic theory and applications. This is an open access, on-line journal PIER (E-ISSN 1559-8985). It has been first published as a monograph series on Electromagnetic Waves (ISSN 1070-4698) in 1989. It is freely available to all readers via the Internet.

PIER is a non-profit organization.

WWW.JPIER.ORG

Contact Email: work@jpier.org

### **Founding Editor in Chief:**

Jin Au Kong, MIT, USA

### **Editors in Chief:**

Professor Weng Cho Chew, University of Illinois at Urbana-Champaign, USA

Professor Sailing He, Royal Institute of Technology, SWEDEN; JORCEP, Zhejiang University, CHINA

**Progress In Electromagnetics Research Symposium**  
**August 1–4, 2018**  
**Toyama, JAPAN**

**PIERS 2018 TOYAMA ORGANIZATION**

**PIERS Chair**

Leung Tsang, University of Michigan

**PIERS 2018 Toyama General Chair**

Kazuya Kobayashi, Chuo University

**PIERS 2018 Toyama General Co-chairs**

Weng Cho Chew, Purdue University

Sailing He, Royal Institute of Technology; JORCEP, Zhejiang University

Tsuneki Yamasaki, Nihon University

**PIERS 2018 Toyama Technical Program Committee Chair  
and Co-Chairs**

Kazuya Kobayashi, Chuo University (Chair)

Ivan Andronov, St. Petersburg State University (Co-Chair)

Iam-Choon Khoo, The Pennsylvania State University (Co-Chair)

Qing Huo Liu, Duke University (Co-Chair)

Tadao Nagatsuma, Osaka University (Co-Chair)

Yoichi Okuno, South China Normal University; Kumamoto University (Co-Chair)

Motoyuki Sato, Tohoku University (Co-Chair)

Yury Shestopalov, University of Gävle (Co-Chair)

Ari Sihvola, Aalto University (Co-Chair)

Meisong Tong, Tongji University (Co-Chair)

Jan Vrba, Czech Technical University in Prague (Co-Chair)

# Contents

Measurement and Modeling of Multi-frequency Microwave Emission of Soil Freezing and Thawing Processes .....	31
Z-R Relationships for Weather Radar in Indonesia from the Particle Size and Velocity (Parsivel) Optical Disdrometer .....	37
Imaging Plasma Inhomogeneities Using Spatial Wave Field Processing with DWFT Approximation ...	42
Optimal Cavities to Enhance Free-space Matching in Solar Cells .....	48
Parabolic Equation of Diffraction Theory: Why It Works Better than Expected? .....	53
Dipole Field Diffraction by a Strongly Elongated Spheroid in High-frequency Approximation .....	59
Diffraction of TM Polarized EM Waves by a Nonlinear Inhomogeneous Dielectric Cylinder .....	66
Measurement of the Diffraction Coefficient of a Trihedral Cone with Homogeneous Neumann Boundary Conditions .....	71
Heterogeneously Integrated Optoelectronic Devices for Implantable Neural Interfaces .....	78
A High-speed Pipelined ADC Based on Open-loop Amplification .....	82
A Chip of Pulse-laser-assisted Dual-beam Fiber-optic Trap .....	86
Rotation of a Trapped Microsphere in a Misaligned Dual-beam Optical Tweezer .....	92
Linear Cellularization Enabling Millimeter-wave Train Radio Communication Systems in 5G Era .....	99
Improvement in Accuracy of Breakpoint Distance Model for Path Loss Prediction .....	107
Effects of Storm Attenuation over Satellite Links in Sub-tropical Africa .....	115
A Comparative Study of Dual-slope Path Loss Model in Various Indoor Environments at 14 to 22 GHz	121
An Empirical Approach to Omnidirectional Path Loss and Line-of-sight Probability Models at 18 GHz for 5G Networks .....	129
The Second Order Moment Equation of Crossly Polarized EM-waves Due to Depolarization in Propagation through Continuous Isotropic Random Medium .....	137
Guided-mode Resonance in Waveguide Cavity .....	144
Microwave Interstitial Applicator Array for Treatment of Pancreatic Cancer .....	150
Microwaves in Medical Diagnostics and Treatment .....	155
Numerical Study of Stroke Detection Using UWB Radar .....	160
Prediction of Cement-based Materials' Water Content with the Use of Electromagnetic Homogenisation Schemes .....	164
Radar Bistatic Configuration for Soil Moisture Estimation at L-band Using Global Sensitivity Analysis Method .....	169
Two-slab High Sensitivity Technique for Measurement of Permittivity of a Dielectric Slab in a Rectangular Waveguide .....	176
Shape Measurement Based on Combined Reduced Phase Dual-directional Illumination Digital Holography and Speckle Displacements .....	184
A- $\Phi$ Formulation Time Domain Integral Equations Free from Interior Resonances .....	190
MOD Based Discontinuous Galerkin PMCHW Method for Simulating Transient Scattering Characteristics of Dielectric Objects .....	197

Characteristic Parameter Estimation of Chipless RFID Signals Based on USRP .....	381
NDF and On-axis Resolution of an Axicon in Near Zone: Numerical Experiments .....	386
On the Number of Independent Equations in Phase Retrieval Problem: Numerical Results in Circular Case .....	392
Programmable Pulse Processor Using Cascaded Microrings on Silicon Photonic Circuits .....	396
WT-based Data-length-variation Technique for Fast Heart Rate Detection .....	399
Transmission Line Analogy for Wave Propagation in Graphene-based Structures .....	405
Emulating Tunneling with Elastic Vibrating Beams .....	410
Design of RFID Tag Antenna Based on the Cole-Cole Model of Human Abdomen .....	414
Characteristics of 340 GHz Slow Wave Structure for Staggered Double-vane Traveling Wave Tube .....	420
Design and Modeling of Tunable Band-stop Filter Using Evanescent Mode Resonators .....	424
An Example of Notch Filter Design Spec for the IM Noise Signal Cancellation in 800 MHz CDMA Frequency Band .....	428
Influence of Tropospheric Ducts on Radio Propagation over Sea Surface .....	432
Mode Absorption Filters Based on Graphene-on-silicon Waveguides .....	437
Optical Force for Particle Trapping in a Nanobeam Photonic Crystal Cavity .....	440
Analysis of Interferogram Phase Noise by Bi-static Data Sets of TerraSAR-X .....	444
Modified Helical Coils Structure for Uniform Magnetic Flux Density .....	449
A Low-profile Antenna Design for LTE/WWAN Smartphone Application .....	454
Eutrophication Analysis of Water Reservoirs by Remote Sensing and Neural Networks .....	458
Filtered Back Projection and Simultaneous Algebraic Reconstruction Technique for Image Formation on Square-shaped Physical Phantom Aimed at Microwave Imaging Applications .....	464
Estimation of the Energy Characteristics of a Multi-position Radar System for the Control of Small-sized Space Debris for Various Orbital Zones .....	470
Estimation of the Resolution of a Multi-position Radar for the Control of Small-sized Space Debris Objects That Are Not Resolved by Angular Coordinates .....	476
Efficient Electromagnetic Scattering Analysis for Multi-scale Problems Using Green's Functions of Arbitrary Scatterers .....	482
Plasmonic Properties of Electrolytes beyond Classical Nanophotonics — A Two-fluid, Hydrodynamic Approach to Nonlocal Soft Plasmonics .....	490
Modeling the Magnetic Field Radiated from a Ferrite Rod Antenna for Mining Proximity Detection Systems .....	496
A Novel Approach to Microfabrication of Planar Microstrip Meander-line Slow Wave Structures for Millimeter-Band TWT .....	506
Radiation Pattern Inspection of the FMCW Signal Using Asynchronous Electro-optic Measurement System .....	510
Novel Measurement Set-ups of FTB Stress Propagation in an IC .....	513
Speed of Light in Vacuum in the Case of a Lumped Electric Circuit .....	520
Numerical Models of a Multilayered Graphene Structure .....	527
Algorithms to Detect and Localize the Source of a Wideband Pulse Signal .....	533
A Numerical Analysis of a Periodic Resonant Structure at THz Frequencies .....	537
Vision-based and Differential Global Positioning System to Ensure Precise Autonomous Landing of UAVs .....	542
High Frequency Scattering from Conducting Rectangular Cylinder via Surface Equivalence Theorem ..	547
<i>H</i> -polarized Plane Wave Diffraction by Thick Conducting Slits .....	553

An Enhanced Model for the Analysis of Non-uniform Multiconductor Transmission Lines Based on Scattering Theory .....	559
Spatial Prediction of Electromagnetic Fields Using Few Measurements .....	565
Coupling of Differential and Common Modes of Two-line Circuits in the Multi-conductor Transmission-line Theory Including Radiation .....	570
Orbital Angular Momentum Generation Using Composite Quasi-continuous Metasurfaces with Perfect Efficiency .....	575
Giant Nonlinear Response of Subwavelength Dielectric Resonators Enhanced by Bound States in the Continuum .....	580
Metasurfaces for Improvement Magnetic Resonance Imaging Characteristics: Novel Designs and In Vivo Studies .....	585
Characterization of Terahertz Plasmonic Structures Based on Metallic Wire Woven Meshes .....	588
Helicity-induced Multifunctional Devices Based on Hybrid Metasurfaces .....	592
Integrated Circuits Using Photonic-crystal Slab Waveguides and Resonant Tunneling Diodes for Terahertz Communication .....	599
Improved Detection Strategies for Nonlinear Frequency-division Multiplexing .....	606
Open Area Concealed Weapon Detection Sensor System Development .....	611
Design and Analysis of Inductive Reluctance Position Sensor .....	621
Wireless Energy Harvesting in RFID Applications at 5.8 GHz ISM Band, a System Analysis .....	627
A Novel Microwave Applicator for Sandy Soil Disinfection .....	636
Study of Simultaneous Switching Noise in Two-dimensional Transport Theory including Radiation Effect .....	642
Effect of Absorbing Coating on Shielding Effectiveness of Electromagnetic Shielding Fabric .....	648
Optimal Design of Yagi Microstrip Antenna Based on Particle Swarm Optimization with Fitness Estimation .....	653
Analysis of Singular-point Generating Mechanisms Based on the Correlations among the Parameters in Coherency Matrix and Those in the Optimized Scattering-mechanism Vector in PolInSAR .....	661
Imaging Performance of Backward and Forward Bistatic SAR .....	669
Adaptive Subsurface Visualization System Using Phase Retrieval Method and Complex-valued Self-organizing Map .....	677
Influence Analysis of Uneven Surface on Landmine Detection Using Holographic Radar .....	683
A 3.5–8 GHz Analog Complex Cross-correlator for Interferometric Passive Millimeter-wave Security Imaging Systems .....	692
Shuffled Structure for 4.225 GHz Antireflective Plates: A Proposal Proven by Numerical Simulation ...	700
A Modified Method for Measuring the Faraday Rotation Angle .....	706
Data Augmentation Using Conditional GANs for Facial Emotion Recognition .....	710
An Efficient Face Recognition Algorithm Based on Deep Learning for Unmanned Supermarket .....	715
Efficient Data Record System for Radio Backend .....	719
Pre-processing VDIF Data in FPGA .....	723
A Novel Extraction Method for Melodic Features from MIDI Files Based on Probabilistic Graphical Models .....	729
Model Calculations for Hardware Correlator at SHAO .....	734
Waveguide BPF Composed of Dielectric Frequency Selective Structure with High Suppression of Spurious Mode .....	739
Design Optimization of RF-MEMS Based Multiband Reconfigurable Antenna Using Response Surface Methodology .....	743

Indoor Localization System Using Commensal Radar Principle .....	751
An Improved Successive-cancellation Decoding Algorithm for Polar Code Based on FPGA .....	756
Improved Electromagnetic Compatibility Design for Printed Circuit Board of Automobile Atmosphere Lamp .....	760
Next Approach of HEMS WPT .....	765
Numerical Study of Hyperthermia Applicator System for Tumor Treatment in Head and Neck Region .....	770
An Interference EMG Model of Selected Water Samples .....	775
Algorithms for Flying Object Detection .....	782
Formation of Ray Trajectories of HF Radiowaves in Midlatitude and Highlatitude Ionosphere during Halloween Storm 2003 According to Radiotomography Data .....	787
Multiple-bounce Modeling of High-rise Buildings with Airborne Tomography Array .....	791
The Study of Composite Scattering from the Target over a Randomly Rough Surface Using SAR/ISAR Imaging .....	797
Scattering Characteristics of Vortex Electromagnetic Waves for a Wedge .....	801
Application of the RK4IP Method for the Numerical Study of Noise-like Pulses in Supercontinuum Generation .....	805
Numerical Analysis of Chaotic Dynamics Produced in a Photonic Crystal Fibers .....	810
Classification and Properties of Modes in Bragg Fibers .....	814
Inverse Synthetic Aperture Ladar Imaging Algorithm for Space Maneuvering Target Using Synchrosqueezing Short-time Fourier Transform .....	819
Analysis of Spectrum Properties of Integrated Optical Chips Applied on IFOG .....	827
Semi Circular Printed Monopole Antenna with $\cup$ Shaped Slot for UWB Applications .....	833
Design of 5 Way Wide Band Wilkinson Power Divider for 6 to 18 GHz Applications .....	838
Magneto-optical Properties of a Magnetic Fluid in the THz Frequency Range .....	843
Multiband Circularly Polarized Synthetic Aperture Radar (CP-SAR) Onboard Microsatellite Constellation .....	848
Comparison Design of X-band Microstrip Antenna for SAR Application .....	854
Gain Enhancement of C Band Linearly-polarized Microstrip Antenna with Square Parasitic Patch for Airborne LP-SAR Sensor .....	858
Dual-band Circularly-polarized Microstrip Antenna for Nano Satellite .....	864
3D Printed Wideband Circularly Polarized Pyramidal Horn Antenna .....	868
Unidirectional Radiation and Gain Enhancement of Circularly Polarized Printed Slot Antenna by Several Shapes of Reflector .....	872
An 8-channels FPGA-based Reconfigurable Chirp Generator for Multi-band Full Polarimetric Airborne/Spaceborne CP-SAR .....	876
An PC-based Airborne SAR Baseband System .....	882
Numerical Solution for Received Power Estimation in a Wave Propagation — A Case of Ground Based C-band SAR Test .....	889
Indoor Experiment of SAR Interferometry with 79 GHz MIMO Sensor .....	894
Single Post-event PolSAR Data Based Earthquake/Tsunami Damage Information Extraction in Urban Areas .....	899
Interferometry Synthetic Aperture Radar (InSAR) Application for Flood Area Detection Observed by Sentinel 1A .....	905
Multi-temporal Land Deformation Monitoring in V Shape Area Using Quasi-Persistent Scatterer (Q-PS) Interferometry Technique .....	910



# Multi-temporal Land Deformation Monitoring in V Shape Area Using Quasi-Persistent Scatterer (Q-PS) Interferometry Technique

Pakhrur Razi<sup>1,2</sup>, J. T. S. Sumantyo<sup>2</sup>, Daniele Perissin<sup>3</sup>, Fajar Febriany<sup>1</sup>, and Yuta Izumi<sup>2</sup>

<sup>1</sup>Physics Department, Universitas Negeri Padang, Sumatra 25131, Indonesia

<sup>2</sup>Center for Environmental Remote Sensing, Chiba University, Chiba 236-8522, Japan

<sup>3</sup>Lyle School of Civil Engineering, Purdue University, West Lafayette, IN 47907, USA

**Abstract**— Kelok Sembilan area, West Sumatra, Indonesia located in ‘V’ contour shape is playing an important role to support the transportation connection in the center of Sumatra. However, in the rainy season, landslide event was high along this way, then monitoring and mapping a necessity to for minimizing its impact. Quasi-Persistent Scatterer Interferometry (Q-PSI) technique was applied for extracting information of land deformation on the area from time to time. Beside have high performance for detecting land deformation, Q-PSI technique was selected to improve the number of PS point. It’s required because the method applied to vegetation area with short wavelength SAR (C-Band). This research was supported by 90 scenes of Sentinel-1A taken from October 2014 to November 2017 for ascending and descending orbit. Both satellite orbits detected two critical location of land deformation namely as zone A and Zone B located in steep slope that more than 500 mm movement in the line of sight (LOS).

## 1. INTRODUCTION

Located in steep slope and high rainfall intensity area [1], the Kelok Sembilan flyover (Fig. 3) with the latitude of  $0^{\circ} 4' 13.30''$  S and longitude of  $100^{\circ} 41' 53.56''$  E West Sumatra, Indonesia is necessary to monitor. This crucial because the Indonesia government has categorized the area into middle and high land movement [2]. Furthermore, almost every year landslide occurs along this way. On March 3, 2017, was large-scale landslide incident in West Sumatra-Riau connection, which was 64 locations of landslide occurrence, two of them on Kelok Sembilan flyover [3]. Monitoring requires obtaining the scientific information about land movement and its critical places from time to time.

Persistent Scatterer Interferometric (PSI) Synthetic Aperture Radar (SAR) have proven effective and reliable technique for measuring multitemporal land deformation on earth surface by investigating point-like radar target during acquisition time. Also, the method can observe wide range deformation area in both subsidence and uplift. Some application applied PSI technique to earth observation such as seismic fault [4], coastal sedimentation monitoring [5], volcanos [6], landslide [7] with accuracy 1 m for height and 1 mm in displacement. However, when classical PSI-SAR technique applied in the non-urban area, the number of permanent scatterer target is low [7,8]. To overcome the problem distributed scatterer target considered to be extracted then the number of PS point distribution on spatial can be improved. The technique is Quasi-Permanent Scatterer Interferometry (Q-PSI) SAR. Processing using PSI and Q-PSI SAR technique relatively equal. However, there are three points has adjusted namely [8]. 1). The images of the dataset are not correlating with one master images 2). Displacement and height of target exploiting from partial coherent target subset of the interferogram. 3). Spatial filtering applied to extend the signal-to-noise ratio.

In last research, observation on the area used the ALOS PALSAR (L-band) for ascending orbit with HH polarization only [7]. However, in this experiment are continuing the inspection with applying short wavelength (C-band) that observed in both ascending and descending orbit.

The objectives of the research are to map and monitor land deformation in “V” shape area using Q-PSI SAR technique observed by Sentinel-1A. The result projected on the ground using google earth with KML format.

## 2. STUDY AREA AND SATELLITE DATASET

Kelok Sembilan area located in Lima Puluh Kota district, West Sumatra, Indonesia. It has been the primary road which is playing an essential role in supporting economic and transportation in center of Sumatera island. The area recorded as a high land movement [3] due to topography

and geology. The ranges of topographical slope in both positive and negative are between  $50^{\circ}$ – $75^{\circ}$  and  $34^{\circ}$ – $70^{\circ}$  respectively [7]. Based on geology survey at least two shapes of fault around Kelok Sembilan area namely normal fault and strike-slip fault. Also, the rock structure is shared-joint constructed of metamorphic rock and sedimentary rock. The complexity of geology condition in the area leads to the high probability of landslide occur. In three recent years from 2015–2017, 110 locations of a landslide along the area connection between West Sumatra and Riau Province [9]. Studying and monitoring a characteristic of land deformation in the area is a necessity as scientific information for preventing and early warning for government and resident.

For monitoring land deformation at the Kelok Sembilan area, 36 and 54 scenes ascending and descending orbit of Sentinel 1A C-band SAR satellite was extracted respectively. The acquisition time of data was taken from October 2014 to 7 December 2017. Both orbits of the satellite were selected to achieve the information in different view of line-of-sight (LOS). Also, to identify the consistency of land deformation zone detection. The track orbit of satellite Sentinel-1A is shown in Fig. 1.

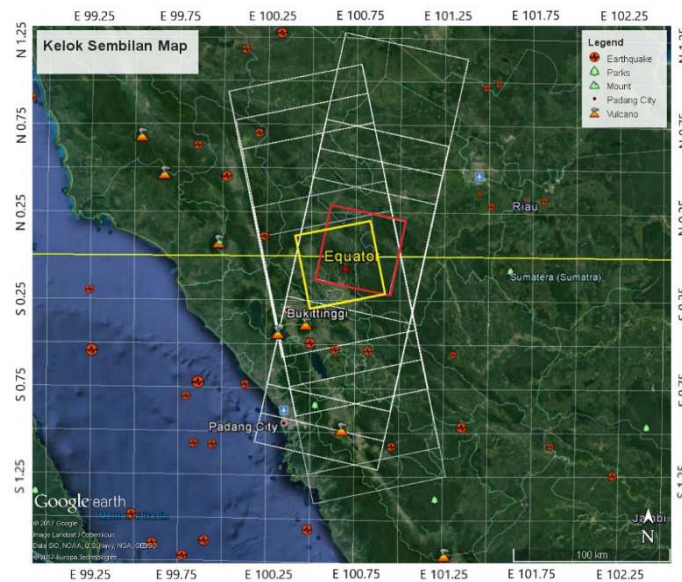


Figure 1: Sentinel-1A satellite with ascending and descending orbit. The yellow square is ascending and red square observation. Kelok Sembilan located near the equator line (yellow line) at a latitude of  $0^{\circ} 4' 13.30''$  S and longitude of  $100^{\circ} 41' 53.56''$  E.

The polarization of SAR data is VV (vertical transmit and vertical receive) with wavelength is 5.44 cm (C-band) and Interferometric Wide (IW) swath mode. The data is provided by European Space Agency (ESA) in single look complex (SLC) product containing phase and amplitude information. Incidence angle radar to target for ascending and descending orbit is 43.39 degree and 43.89 degrees respectively. In an IW SLC product include one image per sub-swath and one per polarization with  $5\text{ m} \times 20\text{ m}$  spatial resolution. The critical baseline for satellite Sentinel-1A is 15,882 m. The orbit height is 693 km with inclination angle  $98.18^{\circ}$  and repeats cycle orbit 12 days [10]. The dataset of Sentinel-1A is shown in Table 1.

Sentinel-1A satellite in both ascending and descending orbit have small the normal baseline. The maximum baseline of the scenes is 200 m. The lower normal baseline will reduce the geometrical decorrelation [11]. Furthermore, the short repeat cycle orbit decreases the temporal decorrelation. Sentinel-1A has both criteria which are small normal baseline and short repeat cycle orbit within 12 days [12].

### 3. METHODOLOGY

#### 3.1. Quasi-Persistent Scatterer (Q-PS) Interferometry Technique

Quasi-Persistent Scatterer Interferometry (Q-PSI) technique is advanced of classical PSI technique that allows extracting the information from partially coherence targets  $\gamma$ . The basic idea of the technique is to improve the spatial distribution of measure points [13]. Q-PSI technique is not only qualified in an urban area but also in the vegetated area, that can improve the spatial density

Table 1: Sentinel-1A with ascending and descending orbit dataset: part 91 frame 592 and path 69 frames 1181 respectively.

No	Orbit	The number of Scenes	Beam swath mode	Acquisition time	Polarization	Off-nadir angle
1	Ascending	36	IW	October 2014– March 2017	VV	35.35°–40.40°
2	Descending	54	IW	October 2014– November 2017	VV	35.35°–40.40°

of Persistent Scatterer Candidate (PSC) [14]. Kelok Sembilan is a vegetated area that has high topography, then the number of PS target is low while observed by C-band than L-band. This is because the number of PSC is correlate with the radar wavelength  $\lambda$ . To do so, Minimum Spanning Tree (MST) image graph configuration with coherence as weight was applied to maximize the coherence target  $\gamma$ . Three components of the image graph considered to improve the coherence target namely: first, the connectivity of image, this needed to unwrap the phase time series. Second, the number of the link. Third, the weight to each link in order to quantify its goodness [8]. The minimum number of image links for  $N$  image available is  $N/2$  and maximum is  $N(N-1)/2$  [13]. Q-PSI technique with MST image graph configuration shown in Fig. 2.

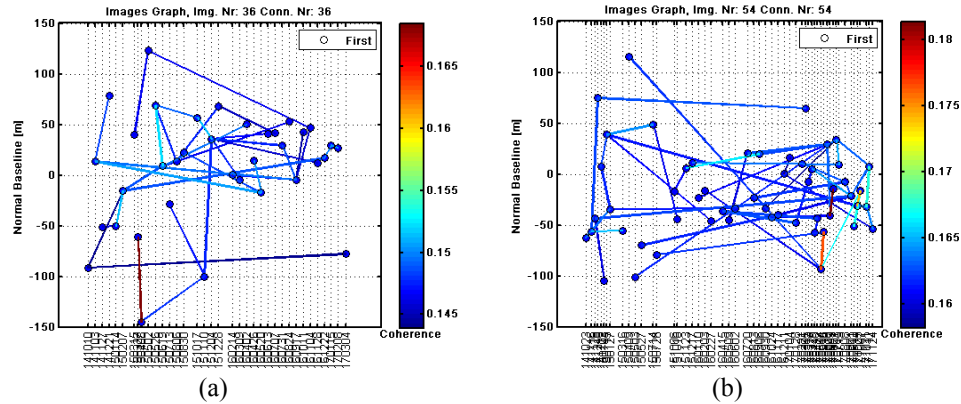


Figure 2: MST image graph configuration for Sentinel 1A SAR satellite in Q-PS technique. (a) Ascending orbit with 36 total number of SAR images. (b) Descending orbit supported by 54 SAR images.

Estimating the atmospheric phase at the pixel position in all interferogram is carried out by selecting the Persistent Scatterer Candidate (PSC) based on amplitude stability index (ASI), ( $ASI = 1 - D_a$ ). The amplitude depression  $D_a$  [15].

$$D_a = \frac{\sigma_a}{m_a} \quad (1)$$

where  $\sigma_a$  the temporal standard deviation of the amplitude value and  $m_a$  the temporal mean of the amplitude value. The point are selected as PSC if the amplitude depression  $D_a < 0.4$  [15, 16]. With minimum PSC density 3 PCS/km<sup>2</sup> [17].

For analyzing full target area, the close point of PSC selection connected each other which refer to the single reference point. The network followed the Delaunay triangulation algorithm [18]. This approach creates more redundancy network to improve the ability to detect the phase ambiguity errors and the robustness of the network.

#### 4. RESULT AND DISCUSSION

Investigation of land deformation in this research is based on the Quasi-Persistent Scatterer Interferometry SAR technique. The data processing was provided by ESA Sentinel 1A satellite in ascending and descending orbit. The time acquisition was taken from October 2014 to March 2017

to October 2014 to November 2017, respectively. For preliminary geocoding and removing the topographic phase component, Shuttle Radar Topography Mission (SRTM) Digital Elevation Model with one arcsec resolution was applied. Furthermore, Amplitude Stability Index (ASI) was used to estimate the preliminary parameter and Atmospheric Phase Scene (APS) through Permanent Scatterer Candidate (PSC) network with threshold 0.6. In both ascending and descending orbit with area range and azimuth  $220 \times 600$  pixel and  $220 \times 900$  pixel, 2136 PSC and 3320 PSC was selected, respectively.

The main component result of Q-PS processing is velocity and height of PS point which represented the condition of the land surface. For Ascending and descending orbit, land deformation velocity around Kelok Sembilan area shown in Fig. 3(a) and Fig. 3(b). In both track orbit, most PS points analyzed locating on a high steep slope and high elevation (Fig. 3(b)) also its PS density. However, in the valley area, the density of PS point is low because the platform is moving parallelly with the terrain. The topography slope more than the off-nadir angle ( $\theta 35.35^\circ\text{--}40.40^\circ$ ) blocked (shadow) the satellite signal then cannot penetrate the valley. Meanwhile, for descending orbit PS density higher than ascending orbit because the satellite slightly crosses topography then some

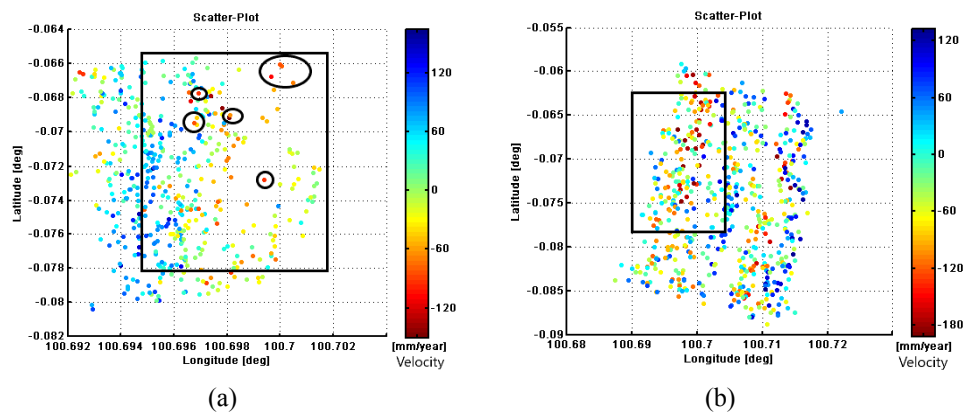


Figure 3: Land deformation velocity for (a) ascending and (b) descending orbit which indicates by color in mm units per year. Persistent scatterer point plotted in geographic coordinate Latitude and longitude with the maximum velocity is more than 120 mm/year (red color). The data observed by Sentinel 1A with 36 and 54 number of scenes from October 2014 to March 2017, respectively.

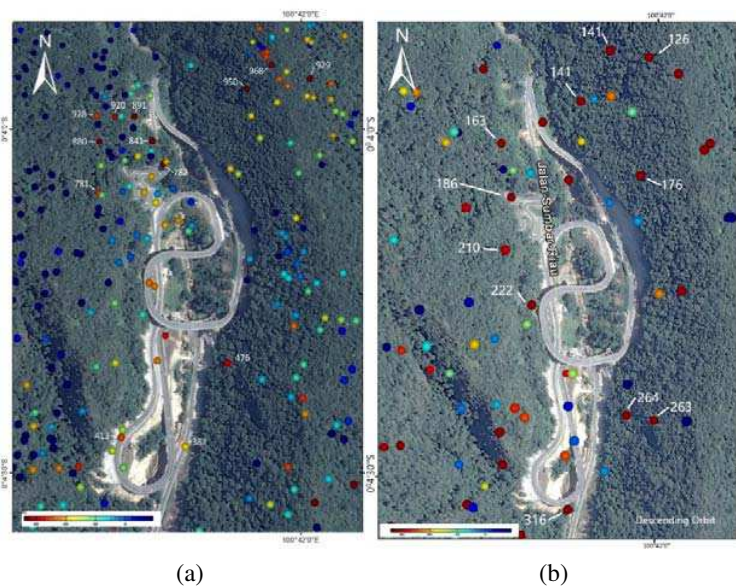


Figure 4: Land deformation area in Kelok Sembilan observed by Sentinel 1A for both ascending and descending orbit. (a) Cumulative displacement of land deformation geocodes into Google Earth for ascending orbit co-polarization (VV). (b) Observed with descending orbit co-polarization. The acquisition time is taken from October 2014 to March 2017 with 90 total number of scenes.

signal reach some area in the valley. For the area,  $1.5 \times 0.97 \text{ km}^2$  which covered by vegetation, 474 PS, and 684 PS detected with temporal coherence  $\gamma > 0.8$  in ascending and descending orbit, respectively. This is high quality value for estimate the height and velocity. The maximum velocity in this observation is more than 120 mm/year and 180 mm/year (red color) during time acquisition for both orbit respectively.

For real visualization land deformation, the PS point geocoded into an optical layer of Google Earth shown in Fig. 4(a) and Fig. 4(b).

For both ascending and descending orbit there are five areas was detected as land deformation consistently. Two of them is crucial because it has higher velocity and larger covered area. The first area represented by ID (476, 264, 263) and the second area by ID (960, 968, 929, 141, 126, 132) where is both zones located on a steep slope. The land deformation maximum for both first and second zones is more than 250 mm and 500 mm in LOS respectively.

## 5. CONCLUSION

In this paper, we show how Q-PS technique can successfully extract the SAR data of Sentinel-1A (C-band) for detection land deformation in V counter shape area. Also, we compared and overlapped the result from ascending and descending orbit observation. There is two location has detected land deformation with a cumulative displacement more than 250 mm and 500 mm with a velocity more than 120 mm/year.

## ACKNOWLEDGMENT

The authors would like to thank Chiba University Excellent International Student Scholarship, KEMENRISTEK DIKTI, Universitas Negeri Padang, ESA Europe, JAXA Japan, SARPROZ, NASA, BNPB, BMKG-SUMBAR.

## REFERENCES

1. BMKG, "Rainfall intensity," 2014–2018, [Online] Available: <http://dataonline.bmkg.go.id/mcstation.metadata>, Accessed: Jan. 20, 2018.
2. Razi, P., J. Tetuko, S. Sumantyo, D. Perissin, and A. Munir, "Persistent scattering interferometry SAR based velocity and acceleration analysis of land deformation: Case study on kelok sembilan bridge," *TSSA IEEE Conf.*, 9–12, 2017.
3. BNPB, "Data and disaster information of Indonesia," <http://dibi.bnpb.go.id>, 2017M [Online] Available: <http://dibi.bnpb.go.id/data-bencana/lihat-data>.
4. Colesanti, C. and J. Wasowski, "Investigating landslides with space-borne Synthetic Aperture Radar (SAR) interferometry," *Eng. Geol.*, Vol. 88, Nos. 3–4, 173–199, 2006.
5. Sumantyo, J. T. S., B. Setiadi, D. Perissin, S. Masanobu, P. P. Mathieu, and M. Urai, "Analysis of land deformation velocity using PSI ALOS PALSAR: Impact of coastal sedimentation to future Jakarta giant sea wall and waterfront city," *Proc. 2015 IEEE 5th Asia-Pacific Conf. Synth. Aperture Radar, APSAR 2015*, Vol. 9, No. 5, 516–521, 2015.
6. Hooper, A., P. Segall, and H. Zebker, "Persistent scatterer interferometric synthetic aperture radar for crustal deformation analysis, with application to Volcan Alcedo, Galapagos," Vol. 112, No. B7, 1–21, 2007.
7. Razi, P., et al., "3D land mapping and land deformation monitoring using persistent scatterer interferometry (PSI) ALOS PALSAR: Validated by Geodetic GPS and UAV," *IEEE Access*, Vol. 6, No. 1, 12395–12404, 2018.
8. Perissin, D. and T. Wang, "Repeat-pass SAR interferometry with partially coherent targets," *IEEE Trans. Geosci. Remote Sens.*, Vol. 50, No. 1, 271–280, 2012.
9. BNPB, "Infografis bencana banjir & Longsor di Kab. Limapuluh Kota, Sumatera Barat," 2017, [Online] Available: <http://geospasial.bnpb.go.id/2017/03/08/infografis-bencana-banjir-longsor-di-kab-limapuluh-kota-sumatera-barat/>.
10. ESA, "Interferometric wide swath," Esa 2000–2018, [Online] Available: <https://sentinel.esa.int/web/sentinel/user-guides/sentinel-1-sar/acquisition-modes/interferometric-wide-swath>.
11. Berardino, P., G. Fornaro, R. Lanari, S. Member, E. Sansosti, and S. Member, "A new algorithm for surface deformation monitoring based on small baseline differential SAR interferograms," Vol. 40, No. 11, 2375–2383, 2002.
12. ESA, *Sentinel-1 User Handbook*, ESA Publications, 2013.

13. Perissin, D. and W. Teng, “Repeat-pass SAR interferometry with partially coherent targets,” *Geosci. Remote Sensing, IEEE Trans.*, Vol. 50, No. 1, 271–280, 2012.
14. Perissin, D. and T. Wang, “Time-series InSAR applications over urban areas in China,” *IEEE J. Sel. Top. Appl. Earth Obs. Remote Sens.*, Vol. 4, No. 1, 92–100, 2011.
15. Kampes, B. M., *Radar Interferometry*, Vol. 12, Springer, The Netherlands, 2006.
16. Ferretti, A., C. Prati, and F. Rocca, “Permanent scatterers in SAR interferometry,” *IEEE Trans. Geosci. Remote Sens.*, Vol. 39, No. 1, 8–20, 2001.
17. Colesanti, C., A. Ferretti, R. Locatelli, G. Savio, I. T. E. T. R. E. S, and V. V Colonna, “Multi-platform permanent scatterers analysis: First results,” 52–56.
18. Ketelaar, V. B. H. G., *Satellite Radar Interferometry: Subsidence Monitoring Techniques*, Springer, The Netherlands, 2009.



公益財団法人

電気通信普及財団

The Telecommunications Advancement Foundation



公益財団法人

Toyama Convention Bureau

富山コンベンションビューロー



公益財団法人 村田学術振興財団

The Murata Science Foundation

